Study of the Frequency Slope Effect on the Chirp Waveform Orthogonality

Leon Kocjancic and Alessio Balleri
Centre for Electronic Warfare, Information and Cyber
Cranfield University
Defence Academy of the United Kingdom
Shrivenham, SN6 8LA, UK
leon.kocjancic@cranfield.ac.uk

Thomas Merlet
Thales Optronique SAS
2 Avenue Gay Lussac
Elancourt, 78990
France

***Abstract*—Multiple-Beam Radar Systems (MBRS) based on waveform diversity require a set of orthogonal waveforms in order to generate multiple channels in transmission and extract them efficiently at the receiver using digital signal processing. Chirp signals are extensively used in radar systems due to their pulse compression properties, Doppler tolerance and ease of generation.**

In this paper, we investigate the level of isolation between two linear frequency modulated (LFM) chirps as a function of the frequency slope and of the chirp starting frequency. Results are derived analytically and verified with a set of measurements at S-band.

I. Introduction

The design of orthogonal waveforms suitable for MBRS, which are based on waveform diversity, is a topic of great interest within the radar research community. Many approaches to find suitable solutions have been investigated in recent years [1]–[3]. One of the techniques proposed to design multiple orthogonal waveforms is to use numerical optimisation algorithms to generate orthogonal polyphase codes [4], [5]. The problem with these is that they are computationally complex, are not Doppler tolerant and they allow a very limited control of the transmitted bandwidth. Another possible technique to achieve orthogonality is to generate noise like stochastic waveforms [6], [7]. However, controlling the waveform bandwidth and the level of Doppler tolerance for these signals is difficult. Previous studies have shown that good orthogonal properties between waveforms can be achieved at the cost of design complexity, spectrum spillage and Doppler intolerance [4], [6].

When designing MBRS with many channels, it is desirable to employ waveforms with chirp-like properties. It is widely known that upchirp and downchirp signals have quasi orthogonal properties and their isolation improves when the time-bandwidth product increases [8]. However, this solution is limited to only two signals with the same bandwidth and duration, and therefore additional waveforms can only be formed with different frequency slopes. This idea was presented in [9] and [10] in order to design orthogonal waveforms based on a saw-like LFM chirp signals for MIMO SAR radars. A methodological approach to investigate orthogonality between LFM chirp waveforms with different frequency slopes and without saw-like frequency modulations has not yet been presented. Our aim is to investigate a radar system with multiple channels, where each channel is assigned with a different task and hence may require different resources. When each task requires a different range resolution $R_r = c/2B$, both the bandwidth and the starting frequency of each channel can be different and slope diversity can be exploited. The main reason to focus on chirp signals is because of their significant advantages over other waveforms, such as range resolution, Doppler tolerance, and implementation simplicity, as noted in [9] and [11].

The goal of this paper is to investigate the isolation between two waveforms as a function of the frequency slope and the chirp starting frequency. A mathematical treatment is presented along with cross-correlation derivations. The theoretical results are validated with a set of simulations and experiments at S-band using software defined radios.

II. Formulation of the Signals

A. Chirp Signal Representation

Let us consider a system that transmits a set of linear chirp signals. The complex envelope of the i-th linear chirp with constant amplitude A_i, starting frequency f_{si} and chirp rate $\mu_i = B_i/T_i$ can be expressed as

$$s_i(t) = A_i \text{rect}\left(\frac{t}{T_i}\right) \exp\left(2\pi j(f_{si}t + \frac{1}{2}\mu_i t^2)\right) \quad (1)$$

where B_i is the bandwidth and

$$\text{rect}\left(\frac{t}{T_i}\right) = \begin{cases} 1, & t \in [0, T_i] \\ 0, & \text{otherwise} \end{cases} \quad (2)$$

is a rectangular function.

B. Cross-Correlation of Chirp Signals

We would like to determine the isolation between a pair of chirps, $s_i(t)$ and $s_j(t)$, by studying the cross-correlation function

$$R_{ij}(\tau) = \int_{-\infty}^{\infty} s_i^*(t) s_j(t+\tau) dt \quad (3)$$

$$R_{ij}(\tau) = A^2 \int_{\eta_1}^{\eta_2} \exp\left(-j2\pi(f_{si}t + \frac{1}{2}\mu_i t^2)\right) \exp\left(j2\pi(f_{sj}(t+\tau) + \frac{1}{2}\mu_j(t+\tau)^2)\right) dt$$
$$= A^2 \exp\left(j2\pi(f_{sj}\tau + \frac{1}{2}\mu_j\tau^2 - \frac{(f_{sj} - f_{si} + \mu_j\tau)^2}{2(\mu_j - \mu_i)})\right) \int_{\eta_1}^{\eta_2} \exp\left(j\pi(\mu_j - \mu_i)(t + \frac{f_{sj} - f_{si} + \mu_j\tau}{\mu_j - \mu_i})^2\right) dt \quad (4)$$

To do this, we assume that the two chirps have the same duration $T_i = T_j = T$, the same amplitude $A_i = A_j = A$ and hence the same energy $E = A^2T$. Different bandwidths, leading to different chirp rates, μ_i and μ_j, and different starting frequencies, f_{si} and f_{sj}, are exploited to study the level of isolation and waveform diversity properties.

Following an approach similar to that in [12], we can analytically express the cross-correlation function with (4). The integration interval $[\eta_1\ \eta_2]$ in (4) depends on τ and can be expressed as

$$[\eta_1\ \eta_2] = \begin{cases} [0,\ T-\tau], & \tau \in [0, T] \\ [-\tau,\ T], & \tau \in [-T, 0) \end{cases} \quad (5)$$

For $|\tau| > T$, $R_{ij}(\tau) = 0$. After a simple change of variable

$$\xi = \sqrt{2(\mu_j - \mu_i)}\left(t + \frac{f_{sj} - f_{si} + \mu_j\tau}{\mu_j - \mu_i}\right) \quad (6)$$

$$d\xi = \sqrt{2(\mu_j - \mu_i)}\, dt \quad (7)$$

the integral in (4) can be expressed more compactly as

$$R_{ij}(\tau) = A^2 K(\tau) \int_{\xi(\eta_1)}^{\xi(\eta_2)} \exp\left(j\frac{\pi}{2}\xi^2\right) d\xi \quad (8)$$

$$= A^2 K(\tau)\left[F(\xi(\eta_2)) - F(\xi(\eta_1))\right] \quad (9)$$

The term $K(\tau)$ can be expressed with (10) and $F(\eta)$ is a complex Fresnel integral defined in (11):

$$K(\tau) = \frac{\exp\left(j\pi\left(2f_{sj}\tau + \mu_j\tau^2 - \frac{(f_{sj} - f_{si} + \mu_j\tau)^2}{\mu_j - \mu_i}\right)\right)}{\sqrt{2(\mu_j - \mu_i)}} \quad (10)$$

$$F(\eta) = \int_0^{\eta} \exp\left(j\frac{\pi}{2}\xi^2\right) d\xi \quad (11)$$

C. Signal Isolation

The isolation $I_{ij}(\tau)$ is defined as the ratio between the maximum amplitude of the autocorrelation function, that is the signal energy E, and the amplitude of the cross-correlation function as

$$I_{ij}(\tau) = \left|\frac{R_{ii}(0)}{R_{ij}(\tau)}\right| = \left|\frac{R_{jj}(0)}{R^*_{ji}(-\tau)}\right| \quad (12)$$

If we insert equation (9) in (12), write $B_i = B_j - \Delta B$, set $f_{sj} = 0$ Hz, and acknowledge that $R_{ii}(0) = E = A^2T$, we can write the isolation for $\tau < 0$ as

$$I_{ij}(\tau)\Big|_{\tau<0} = \sqrt{2T\Delta B}\left[F\left(\sqrt{\frac{2\Delta B}{T}}\left(T + \frac{B_j\tau - f_{si}T}{\Delta B}\right)\right)\right.$$
$$\left. - F\left(\sqrt{\frac{2\Delta B}{T}}\left(-\tau + \frac{B_j\tau - f_{si}T}{\Delta B}\right)\right)\right]^{-1} \quad (13)$$

and this is a contribution of this paper.

A further elaboration of (13) and the plots of the theoretical curves would show that increasing the pulse width T or the bandwidth difference ΔB improves the isolation performance. Such improvements will be corroborated in the experimental section of this paper. It can also be shown that the arguments of the Fresnel integrals $F(\cdot)$ mainly affect the width of the mainlobe and have an additional effect on the maximum value of the isolation due to constructive or destructive contributions of the Fresnel integrals.

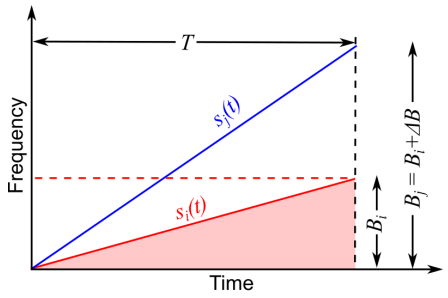

Fig. 1. Frequency modulations of compared chirp signals $s_i(t)$ and $s_j(t)$ with zero starting frequency and ΔB bandwidth difference.

III. Simulation Results

A. Chirp Rate Effect on the Isolation

In this section, we determine the effect of bandwidth differences ΔB on the isolation, given the same pulse width. In the simulations, the initial frequencies were set to $f_{si} = f_{sj} = 0$ MHz, the pulse width to $T = 10\ \mu$s, the bandwidth of $s_j(t)$ was fixed to $B_j = 50$ MHz, and ΔB was varied in order to produce different cross-correlation curves $R_{ij}(\tau)$. The time-frequency diagram, indicating the frequency modulation of the two signals under test, is shown in Fig. 1. Examining the results in Fig. 2, it is evident, that the bigger the bandwidth separation ΔB the better is the suppression of the unmatched chirp signal. When ΔB increases, the sidelobes become longer and extend towards the negative delay of the cross-correlation.

This phenomenon can be explained by looking at the time-frequency characteristics in Fig. 1 and by analysing (4). For a negative value of τ, the frequency curve of $s_j(t)$ moves to the right and starts overlapping the frequency curve of $s_i(t)$. This causes a stronger coupling and results in a larger values of the cross-correlation for $\tau < 0$. For positive values of τ, the frequency slopes are further apart and the amplitude of the cross-correlation drops significantly.

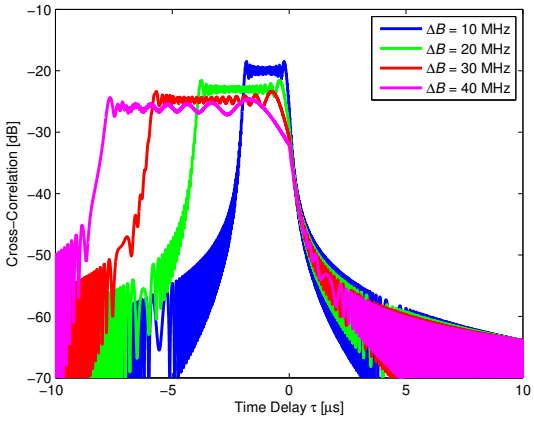

Fig. 2. Simulated absolute value of cross-correlation functions for chirp signals $s_i(t)$ and $s_j(t)$ with different bandwidths. Bandwidth difference is denoted by ΔB and normalisation is done with respect to the autocorrelation peak.

The isolation between the matched and unmatched chirp signals, as given in (12), is shown in Fig. 3. We can observe that the isolation is constantly increasing with the increasing bandwidth difference ΔB.

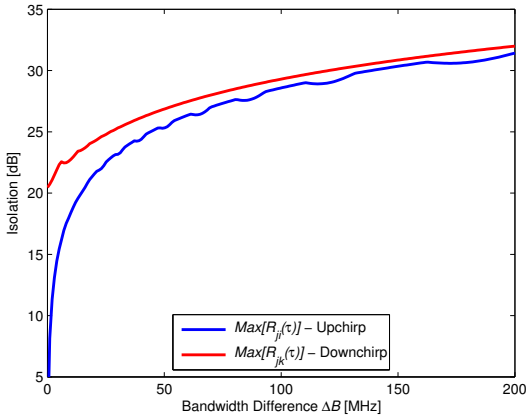

Fig. 3. Simulated isolation between chirp signals as a function of bandwidth difference ΔB. The blue curve shows isolation between upchirps $s_j(t)$ and $s_i(t)$, while the red curve shows relation between upchirp $s_j(t)$ and downchirp $s_k(t)$.

B. Frequency Offset Effect on the Isolation

In this section, we investigate the effect of changing the starting frequency f_{si} of the first upchirp signal $s_i(t)$ on the

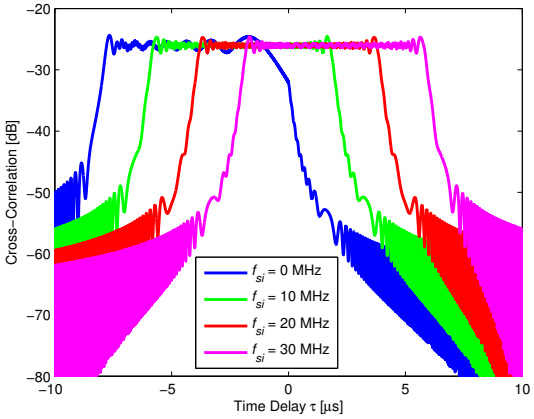

Fig. 4. Simulated cross-correlation function of the two chirp signals with $B_i = 10$ MHz, $B_j = 50$ MHz and $T = 10$ μs. The starting frequency f_{si} is varied as indicated in the legend.

cross-correlation properties when $s_j(t)$ is an upchirp with a different bandwidth. An example of the frequency modulations of both signals are those with a positive chirp rate shown in Fig. 6. In this simulation, the duration of the signals is $T = 10\mu$s, the bandwidth of the first signal is $B_i = 10$MHz and that of the second signal is $B_j = 50$ MHz. The starting frequency of the first chirp is varied from 0 MHz to 30 MHz. The main effect of varying f_{si} is a shift of the cross-correlation peaks along the time delay axis. This phenomenon is depicted in Fig. 4 and it is similar to one introduced in the previous section. Increasing the starting frequency f_{si} results in a greater signal spectrum coupling for $\tau < 0$, which results in a shift of the cross-correlation to the left.

Fig. 5 shows a plot of the isolation as a function of starting frequency for a few values of ΔB. Results show that varying the starting frequency f_{si} has a minor effect on the isolation of both signals after matched filtering. The parametrised bandwidth difference ΔB, in this case, has a much greater impact on the isolation. Fixing B_j to 60 MHz and varying ΔB from 10 MHz to 50 MHz improves the isolation from approximately 18.5 dB to 25.5 dB. On the other hand, the mean value of the isolation is, when $\Delta B = 30$MHz, 23.3 dB and all values fall in the interval between 23.3 dB $\pm$ 0.06 dB.

The results suggest that it could be possible to introduce many frequency displaced chirps with smaller bandwidths that would cause very similar effects on the cross-correlation function.

C. Combining Upchirp and Downchirp Signals

Two chirp signals with the same bandwidth but with increasing and decreasing frequency show a good degree of orthogonality [13]. Their orthogonal property can be exploited together with frequency slope waveform diversity in order to produce more than two channels for a MBRS. The idea is shown in Fig. 6, where a signal $s_j(t)$ coexists with two signals $s_i(t)$ and $s_k(t)$ in the time-frequency domain. The isolation

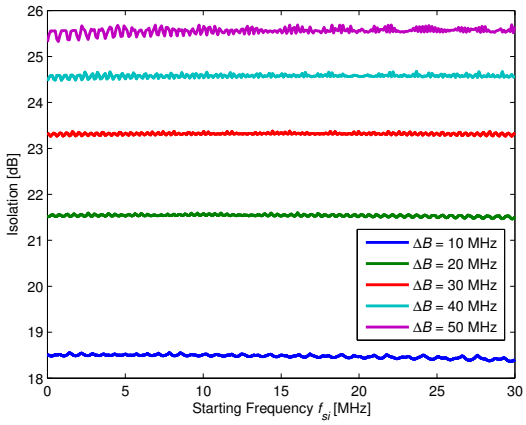

Fig. 5. Simulated isolation levels between chirp signals $s_i(t)$ and $s_j(t)$ with different bandwidth differences ΔB and different starting frequencies f_{si}.

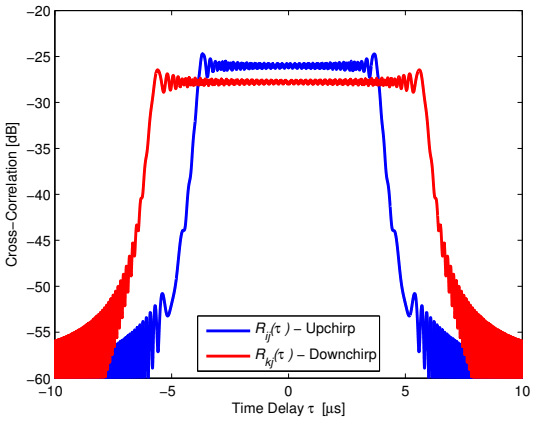

Fig. 7. Simulated isolation for the upchirp signal $s_i(t)$ and downchirp signal $s_k(t)$ with $B_i = B_k = 10\,\text{MHz}$ when compared to wider bandwidth upchirp $s_j(t)$ with $B_j = 50$ MHz.

separation is even better between signals with positive and negative frequency slopes. This can be observed in Fig. 3 where the biggest difference in signal separation occurs for smaller bandwidth differences. Thus, combining upchirp and downchirp waveforms should improve waveform isolation. When the bandwidth difference of the two upchirp signals is small and starting frequency is the same, separation is not possible. In such case, only a combination with a downchirp forms an orthogonal pair.

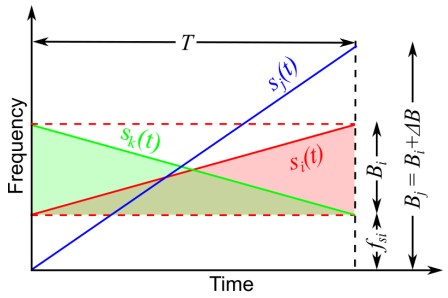

Fig. 6. Frequency modulations of compared upchirp signals $s_i(t)$, $s_j(t)$ and downchirp signal $s_k(t)$ that were used in simulations.

To illustrate the difference, three chirps are compared with frequency modulations according to Fig. 6. The time duration for all signals is $T = 10\ \mu$s, $B_i = B_k = 10$ MHz, $B_j = 50$ MHz and $f_{si} = 20$ MHz. The signal $s_i(t)$ represents a downchirp, $s_k(t)$ is an upchirp, and the signal $s_j(t)$ is an additional upchirp to which both are compared. Fig. 7 shows the resulting cross-correlation functions $R_{ij}(\tau)$ and $R_{kj}(\tau)$. It can be seen that the downchirp $s_k(t)$ has a better isolation with respect to $s_j(t)$ than the upchirp $s_i(t)$. The improvement in isolation amounts to about 2 dB. However, the sidelobes become wider after pulse compression.

IV. Experimental Results

A. Experimental Setup

The prototype consists of a Universal Software Radio Peripheral (USRP) device with two transmitting ports and one receiving port. The two transmitting channels TX1 and TX2 host two identical antennas, while the receiving horn antenna is connected to the receiving channel RX1. A diagram and a photo of the prototype are shown in Fig. 8 and in Fig. 9, respectively.

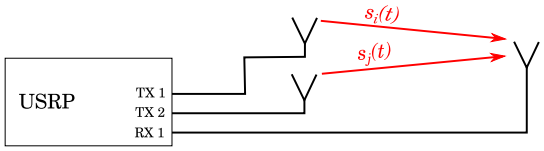

Fig. 8. Schematic diagram of the experimental setup.

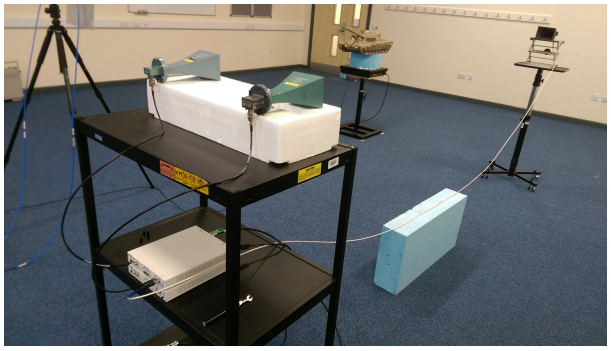

Fig. 9. Photo of the experiment that was conducted using USRP, two transmitting, and one receiving antenna.

B. Experimental Results

The first experiment was carried out with only one active transmitting antenna facing the receiving antenna from a 2

TABLE I
ISOLATION BETWEEN DIFFERENT CHIRP WAVEFORMS

T	Chirp	ΔB			
		10 MHz	20 MHz	30 MHz	40 MHz
10 μs	Up-Up	17.09 dB	20.82 dB	22.77 dB	24.04 dB
10 μs	Up-Dn	26.26 dB	26.91 dB	26.12 dB	25.56 dB
20 μs	Up-Up	19.96 dB	23.97 dB	25.84 dB	27.18 dB
20 μs	Up-Dn	29.35 dB	29.99 dB	29.21 dB	28.69 dB

m distance. The two waveforms under test were transmitted and acquired separately, by running two consecutive measurements, to corroborate the simulation results of the chirp rate effects on the cross-correlation properties. Such approach was selected to allow an accurate measurement of the isolation between different signals. During the experimental work, the sampling frequency was $f_s = 125$ MHz and the carrier frequency was $f_c = 6.0$GHz. The number of transmitted samples was set to 1250, so that the waveform length corresponded to $T = 10$ μs. In receive, 1500 samples were acquired and after that square windowing was applied to extract only the transmitted signal.

The waveform parameters used in the experiment were the same as those of the simulations; the bandwidth of the first signal was kept constant with $B_j = 50$ MHz and that of the second signal was varied according to $B_i = B_j - \Delta B$. The waveform $s_i(t)$ was transmitted and received with the same sampling frequency. A filter matched to $s_j(t)$ was used to process the received signals. The measured results are plotted in Fig. 10 and results corroborate the simulations presented in the previous section. For $\Delta B = \{20, 30, 40\}$ MHz, the difference between the measurements and the simulations is on the average less than 0.5 dB.

Table I presents a summary of the results. It can be observed that increasing the pulse width T improves the isolation ratio I_{ij}. Isolation performance for signals with a constant pulse width are further improved by increasing the bandwidth difference ΔB. The best isolation results were achieved when an upchirp signal s_j was compared to a downchirp signal s_k.

The second experiment was carried out with two active transmitting antennas. Two radar waveforms were simultaneously transmitted and then received with the receiving antenna placed at a distance of 4 m from the transmitter. Fig. 11 shows the results for the case when two waveforms $s_j(t)$ and $s_i(t)$ are transmitted simultaneously and the receiver is matched to $s_i(t)$. Results show the sidelobes of the suppressed signal $s_j(t)$ and the normalised autocorrelation peak at the centre of the plot. For the case with $B_j = 50$ MHz, $B_i = 20$ MHz and $f_{si} = 10$ MHz, the measured isolation was $I_{ij} = 20$ dB.

V. CONCLUSION

This paper presents a study of the orthogonal properties of linear frequency modulated waveforms for MBRS. The mathematical expression of the isolation was derived analytically for chirp signals with different bandwidths and different starting frequencies. The theoretical results were demonstrated using

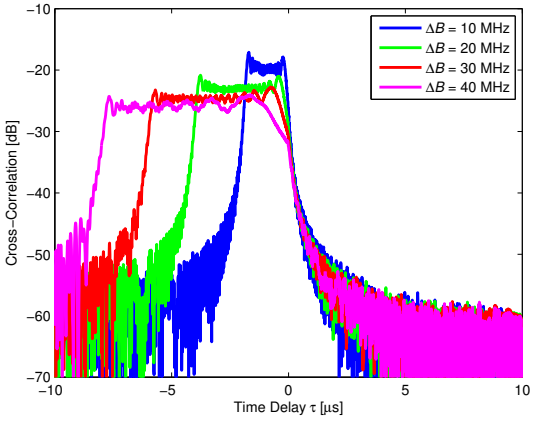

Fig. 10. Experimentally measured absolute values of cross-correlation functions for chirp signals with different bandwidths ΔB.

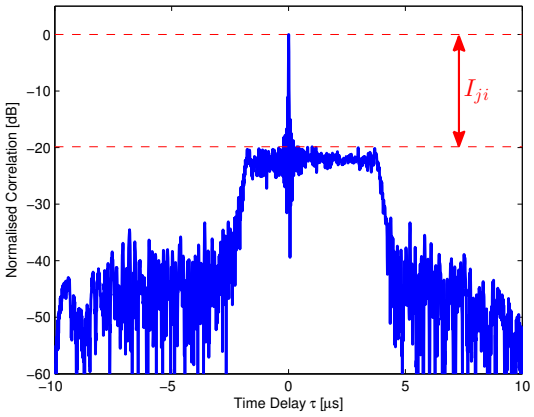

Fig. 11. Experimentally measured isolation between two transmitted upchirp signals $s_j(t)$ and $s_i(t)$ with different bandwidths. The amount of isolation S_{ji} is marked with the red arrow.

simulations and then confirmed with the experimental results. Future work will look at studying the relationship between maximum range, SNR, isolation and Doppler effects between multiple channels of a radar system.

ACKNOWLEDGEMENT

The authors would like to express gratitude to Professor Alfonso Farina for his useful comments, to the MCM-ITP programme and Thales Optronique for funding this research.

REFERENCES

[1] G. Galati and G. Pavan, "Waveforms design for modern and MIMO radar," *Eurocon*, pp. 508–513, Jul. 2013, Zagreb, Croatia.

[2] L. Lo Monte, B. Himed, T. Corigliano, and C. J. Baker, "Performance analysis of time division and code division waveforms in co-located MIMO," *IEEE Radar Conference*, pp. 794–798, Oct. 2015, Johannesburg, South Africa.

[3] M. Cattenoz and P. Brouard, "Coherent collocated MIMO radar: A study on real data," *14th International Radar Symposium*, Jun. 2013, Dresden, Germany.

[4] H. Deng, "Polyphase Code Design for Orthogonal Netted Radar Systems," *IEEE Transactions on Signal Processing*, vol. 52, no. 11, pp. 3126–3135, Nov. 2004.
[5] H. He, P. J. Li, and P. Stoica, "Waveform Design for Active Sensing Systems: A Computational Approach," *Cambridge University Press, Cambridge*, 2012.
[6] M. A. Govoni and H. Li, "Low Probability of Interception of an Advanced Noise Radar Waveform with Linear-FM," *IEEE Transactions on Aerospace and Electronic Systems*, vol. 49, no. 2, pp. 1351–1356, Apr. 2013.
[7] K. Kulpa, "Signal Processing in Noise Waveform Radar," *Artech House, New York*, 2013.
[8] S. Welstead, "Characterization of diversity approaches for LFM stretch-processed waveforms," *International Waveform Diversity and Design Conference*, pp. 418–422, Jun. 2007, Pisa, Italy.
[9] W. Q. Wang, "MIMO SAR Chirp Modulation Diversity Waveform Design," *IEEE Geoscience and Remote Sensing Letters*, vol. 11, no. 9, pp. 1644–1648, Feb. 2014.
[10] Wen-Qin Wang, "Large Time-Bandwidth Product MIMO Radar Waveform Design Based on Chirp Rate Diversity," *IEEE Sensors Journal*, vol. 15, no. 2, pp. 1027–1034, Feb. 2015.
[11] C. E. Cook and M. Bernfeld, "Radar signals: an introduction to theory and application," *Artech House, Boston*, 1993.
[12] Wen-Qin Wang, Qicong Peng, and Jingye Cai, "Waveform-Diversity-Based Millimeter-Wave UAV SAR Remote Sensing," *IEEE Transactions on Geoscience and Remote Sensing*, vol. 47, no. 3, pp. 691–700, Mar. 2009.
[13] G. Galati and G. Pavan, "Orthogonal and Complementary Radar Signals for Multichannel Applications," *8th European Radar Conference*, pp. 178–181, Oct. 2011, Manchester, United Kingdom.